

The Atomistic Study of Textured Polycrystalline Nanofilms

I-L. Chang¹ and W.-C. Ding

Abstract: Molecular dynamics method incorporating with parallel computing technique was employed to study the mechanical properties of textured polycrystalline nanofilms with fixed out-of-plane normal direction. The grain size and film thickness effects on both the elastic and plastic properties of the copper nanofilm were examined. It is shown from the simulation that the elastic and plastic properties (i.e., Young's modulus, Poisson's ratio, biaxial yield stress, etc) of textured polycrystalline nanofilms depend on the grain size and the film thickness. As the grain size of the nanofilm become larger, the Young's modulus and biaxial yield stress increase but the Poisson's ratio decreases. It is observed that both the grain boundary sliding and the dislocation emerging inside the grains are the dominant mechanisms for the plastic deformation and thus, the inverse Hall-Petch effect becomes prominent in polycrystalline nanofilm. Moreover, as the thickness of the nanofilm increases, the Young's modulus increase but the biaxial yield stress does not show clear dependence.

Keywords: Polycrystalline nanofilm, molecular dynamics, elastic constant, grain.

1 Introduction

In recent years, polycrystalline nanofilms have drawn increasing interest in both academia and industries [Tracy and Knorr (1993); Choi and Suresh (2002); Kalkman et al. (2001)]. Metallic polycrystalline nanofilms, grown onto amorphous substrates by almost any deposition method, show at least some degree of crystallographic texture [Tracy and Knorr (1993)], which induces macroscopic anisotropy. The observed texture mostly displays a fiber texture, in which the surface normal of the grains are nearly parallel to a specific crystallographic direction while a random orientation of grains is simultaneously maintained in the plane of the film. With the recent advance of nanotechnology, it provides a unique opportunity to have an in-depth understanding of how the mechanical properties of textured polycrystalline nanofilms depend on the characteristic size of microstructure and the film thickness.

Significant research efforts have been made to investigate the size effects on the mechanical properties of nanofilms including theoretical, experimental methods and molecular simulations. Many experimental techniques have been developed to evaluate mechanical properties of nanofilms, including nanoindentation testing[Ruud et al. (1994); Choi et al. (2003); Son et al. (2003)], x-ray diffraction with in situ tensile testing[Villain et al. (2002); Renault et al. (2003)] and laser-ultrasonic surface acoustic wave spectrometry [Hurley et al. (2001)]. Some experiments[Renault et al. (2003); Yang et al. (1977); Baral et al. (1985); Cuenot et al. (2004)] show the increase in elastic modulus as the constituent film size decreases while other experiments[Ruud et al. (1994); Villain et al. (2002); Hurley et al. (2001); Petersen and Guarnieri (1979)] show the opposite trend.

In addition to experimental characterization, the use of molecular simulations in the study of the mechanical properties of nanomaterials has given unique insight into the atomic scale phenomena that occur during elastic and plastic deformation[Streitz et al. (1990); Diao et al. (2004); Chang and Chen (2007); Yamakov et al. (2001, 2002, 2004)]. However, most of the research focuses on single-crystalline nanomaterials[Streitz et al. (1990); Diao et al. (2004); Chang and Chen (2007)]. Some researchers studied the microstructure size effect on the plasticity behavior of nanocrystalline materials. Yamakov *et al* [Yamakov et al. (2001)] studied the nucleation of dislocations from the grain boundaries in nanocrystalline aluminum using molecular dynamics (MD) simulation. Van Swygenhoven *et al* [Yamakov et al. (2002)] performed constant uniaxial deformation on nickel and copper nanocrystalline bulk using MD simulation and found that the deformation mechanism was function of grain size, which indicated that all deformation is accommodated in the grain boundaries at the smallest grain sizes, while at higher grain sizes, intragrain deformation is observed. Schiotz *et al* [Yamakov et al. (2004)] used MD simulations with system sizes up to 100 million atoms to simulate plastic deformation of nanocrystalline copper and observed that the strength exhibit a maximum at a grain size of 10 to 15 nanometers, which is because of a shift in the microscopic deformation mechanism from dislocation-mediated plasticity in the coarse-grained material to grain boundary sliding in the nanocrystalline region.

Microstructure and film thickness are two important factors influencing the mechanical properties of polycrystalline nanofilms especially when the film thickness and the material microstructures become compatible. In order to take these two factors into consideration, molecular dynamics methods incorporating with parallel computing technique will be employed to study the mechanical behaviors of textured polycrystalline nanofilm in this research. Infinite large nanofilms with various grain sizes and film thicknesses will be loaded in order to thoroughly investigate

the size dependence of both elastic and plastic properties.

2 Molecular Simulation

To carry out molecular simulation, the suitable interatomic potentials and atomic model are required. Without loss of generality, face-center-cubic (FCC) copper is chosen for this study. The microstructure of copper films is of particular interest because of its use in various electronic applications. Embedded-atom-method (EAM) potential first developed by Foiles, Baskes, and Daw [Van Swygenhoven et al. (2001)] is chosen to describe atomic interactions. Among the various types of n -body potentials, the EAM potential is one of the most realistic and promising potentials, which provide a relevant description of the surface effect and defect properties of the transition metals with either an FCC or BCC structure [Schiotz and Jacobsen (2003)]. In EAM potential, the total energy is composed of the electrostatic pairwise interaction energy between atoms and the embedding energy required to insert the atom into the local electron density field created by its near neighbors. Empirical functions in EAM potential are fitted to experimentally measured bulk material properties, such as equilibrium lattice constants, sublimation energies, elastic constants, and vacancy formation energy.

2.1 Atomic Model

The film is assumed to be composed of the hexagonal grains [Yamakov et al. (2001)] with size, d , on the order of nanometers. The arrangements of the grain crystallographic orientations are random with out-of-plane normal direction fixed at the [001] direction [Tracy and Knorr (1993)]. Each hexagonal grain is constructed by rotating the original film with in-plane directions ($X[100]$ and $Y[010]$) by a random angle, θ , as shown in Fig. 1. The rotating angle varies from 0 to $\pi/2$ due to the crystallographic symmetry. The hexagonal grains are assembled together with a gap of 1.6\AA in between to prevent that the atoms at different grains are too close.

The periodic boundary conditions (PBC) are applied on both in-plane x and y directions to simulate an infinite large film. Minimum image criterion is adopted to implement the periodic boundary condition. In order to properly simulate an infinite nanofilm, some attentions need to be paid to the crystallographic orientations of the grains positioning at the perimeter (i.e. the corner and the side) of atomic model. As shown in Fig. 1(b), the orientations of the four corner quarter grains need to be the same. Meanwhile, the orientations of the left and right side of the half grains have to be consistent so as the top and bottom side.

The nanofilms with various grain sizes and film thicknesses are simulated to inves-

condition will be simulated five times with grain orientations randomly chosen in order to achieve the statistical significance.

2.2 Molecular Dynamics Simulation

All simulations are performed at room temperatures, 300K and Newton's equations of motion are solved using a fifth order Gear predictor-corrector algorithm with a 1fs step size. The force acting on an individual atom is obtained by summing the forces contributed by the surrounding atoms. The initial atomic models of polycrystalline nanofilms will be relaxed under NTV ensemble with x, y periodic lengths adjusted so that the in-plane stresses (σ_{xx} and σ_{yy}) are diminished to zero. The out-plane stress (σ_{zz}) will automatically vanish as long as the relaxation time is long enough since there is no constraint or periodic condition applied in z direction. Every adjusted atomic model is relaxed for 10^5 time steps to make sure the nanofilms reach their equilibrium states.

Uniaxial and biaxial strain deformations are loaded on nanofilms to extract their elastic and plastic properties separately as shown in Fig. 2. In order to reduce the loading strain rate, additional MD steps are applied for the relaxation of the nanofilm after each stage of the loading, and the mechanical properties of the relaxed structure are attained. The equilibrated configuration will be used as the initial state for the next loading step. In this study, the applied strain increment is 0.5%, and then the nanofilm system is relaxed for the interval of 10ps, whose corresponding strain rate is $0.05\% \text{ ps}^{-1}$.

3 Results

MD approach combined with parallel computing scheme is utilized to simulate the uniaxial and biaxial loading test of textured polycrystalline nanofilms. The grain size and thickness effects on elastic and plastic behaviors are studied and systematically compared through the stress-strain relation. The atomic structures of the textured nanofilms at the equilibrium are examined and it is found that the initial grain shapes are still preserved with slightly blurred grain boundaries as plotted in Fig. 3. Moreover, the radial distribution functions (RDF) of the equilibrated nanofilms for different grain sizes are depicted in Fig. 4. It is noticed that the polycrystalline nanofilm still remain crystalline fcc structure especially for larger grain size while the RDF starts to exhibit long-range disorder for smaller grains, which indicates that the atoms at the grain boundaries are amorphous without specific crystal structure.

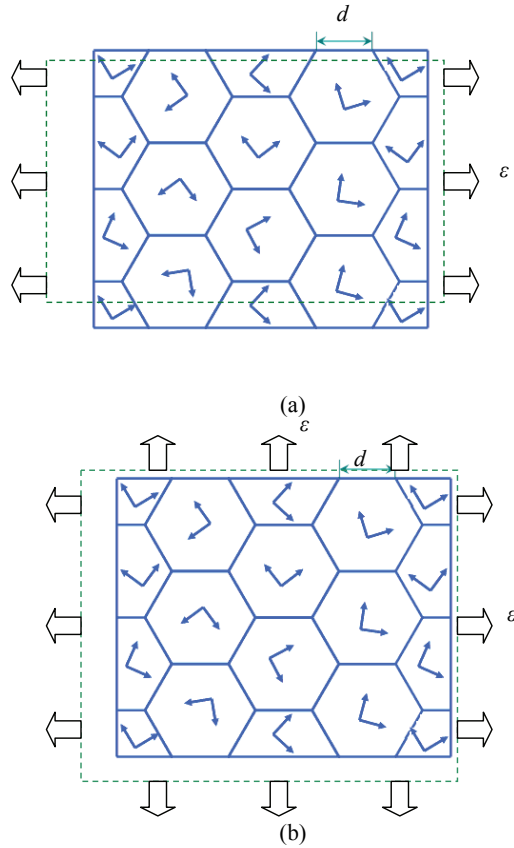


Figure 2: The schematic presentation of the nanofilm under (a) uniaxial loading and (b) biaxial loading

3.1 Elastic Property

Both tensile and compressive uniaxial simple tension loadings are applied along x direction on the equilibrated nanofilm model. Meanwhile, the transverse periodic length needs to be adjusted to cancel the induced stress, σ_{yy} , due to Poisson's effect. However, some significant amount of shear stress, τ_{xy} , still remains while satisfying the plane stress state ($\sigma_{zz} = \tau_{xz} = \tau_{yz} = 0$). In order to maintain the rectangular periodic box formation, the shear stress is induced since only limited numbers of grains could be simulated, in which the distributions of grain orientations would be possibly asymmetric spatially.

Assume the plane elastic properties of the textured polycrystalline nanofilm could

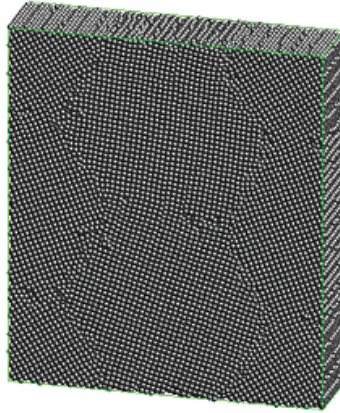


Figure 3: The equilibrated nanofilm model with grain size of 52.18Å and film thickness of 36.15Å

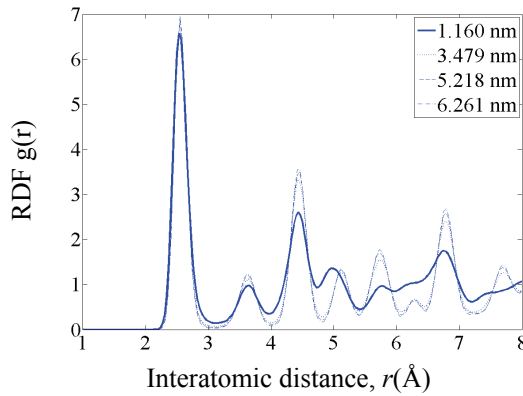


Figure 4: Radial distribution function of textured polycrystalline nanofilms with different grain sizes

be described by general Hook's law as

$$\begin{Bmatrix} \epsilon_{xx} \\ \epsilon_{yy} \\ \gamma_{xy} \end{Bmatrix} = \begin{bmatrix} \frac{1}{E_x} & -\frac{\nu_{xy}}{E_x} & s_{16} \\ -\frac{\nu_{xy}}{E_x} & \frac{1}{E_y} & s_{26} \\ s_{16} & s_{26} & \frac{1}{G_{xy}} \end{bmatrix} \begin{Bmatrix} \sigma_{xx} \\ \sigma_{yy} \\ \tau_{xy} \end{Bmatrix} \quad (1)$$

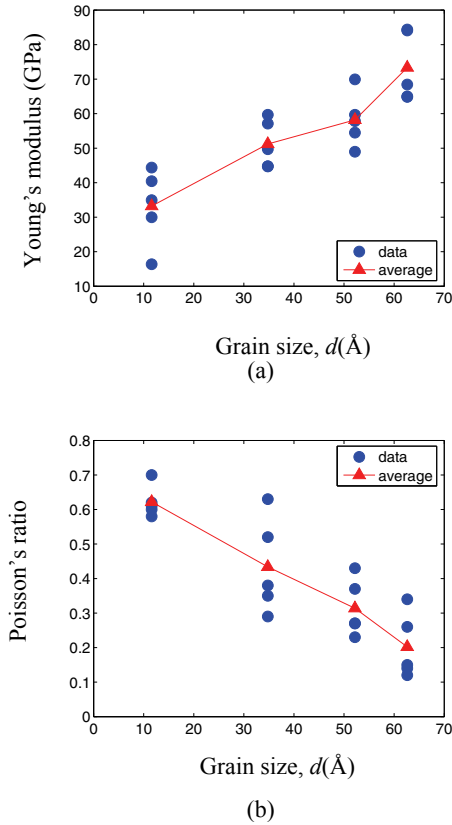


Figure 5: Size dependences of elastic properties on grain sizes of textured polycrystalline nanofilms. (a) Young's modulus, (b) Poisson's ratio.

Under the simple tension/compression condition ($\sigma_{yy} = 0$), the plane stress-strain relation could be rewritten as

$$\epsilon_{xx} = \frac{1}{E_x} \sigma_{xx} + s_{16} \tau_{xy} \quad (2)$$

$$\epsilon_{yy} = -\frac{\nu_{xy}}{E_x} \sigma_{xx} + s_{26} \tau_{xy} \quad (3)$$

Both tensile and compressive loading of 0.5% strain, ϵ_{xx} , are applied on the nanofilm model to attain the stresses (σ_{xx} , τ_{xy}) and transverse strain ϵ_{yy} . Since the loading strain is quite small, it is reasonable to consider that the elastic properties remain constant in this range. Solving these simultaneous linear equations (2) and (3), the

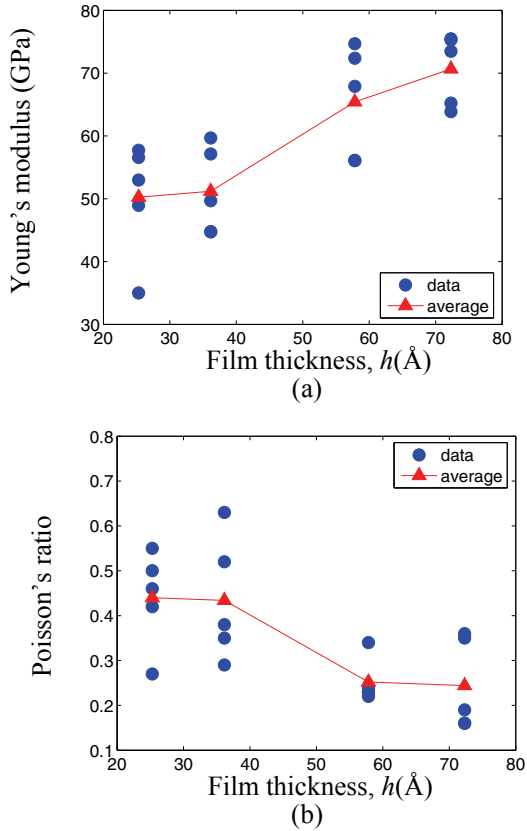


Figure 6: Size dependences of elastic properties on film thicknesses of textured polycrystalline nanofilms. (a) Young's modulus, (b) Poisson's ratio.

Young's modulus and Poisson's ratio of the textured polycrystalline nanofilm could be calculated.

The elastic moduli calculated from MD simulation results for four different grain sizes and film thicknesses of nanofilms are shown in Fig. 5 and 6. It is noticed that the average Young's modulus increases as the grain gets larger and film gets thicker, while the average Poisson's ratio possess opposite trend. It should be pointed out that the scattered data is due to the limited numbers of grains, which could not maintain adequate randomness in the crystal orientations even though the grain orientations are randomly assigned.

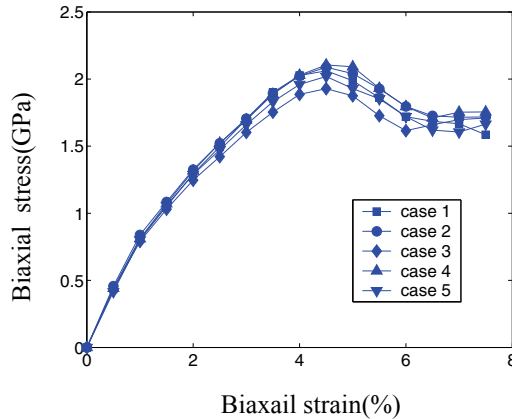
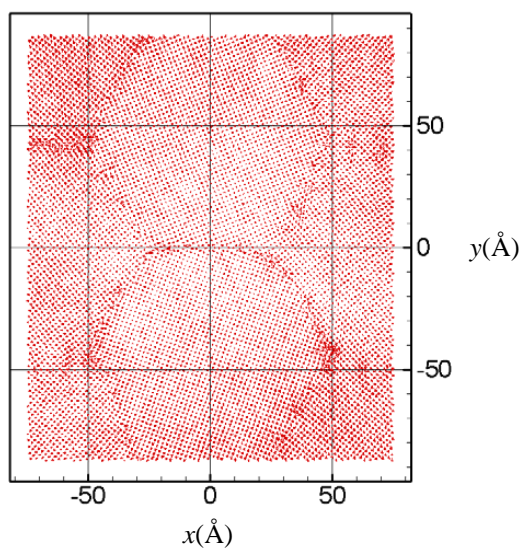


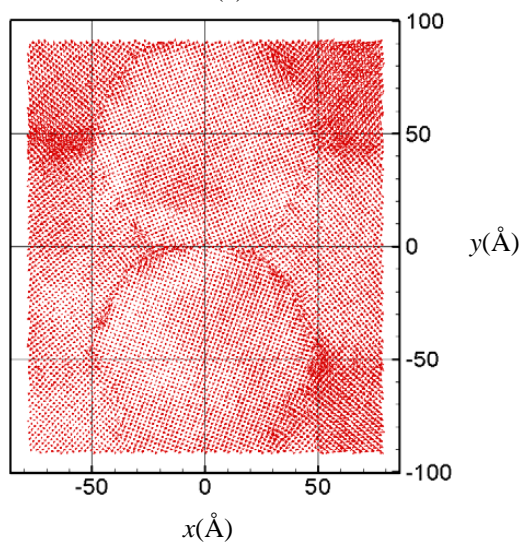
Figure 7: Biaxial stress-strain relations of polycrystalline nanofilm with grain size of 34.79\AA and film thickness of 36.15\AA

3.2 Plastic Property

To study in detail the plastic property, the nanofilms are loaded biaxially beyond the elastic limit. The average biaxial stress-strain curves of textured polycrystalline nanofilm for five different tests are illustrated in Fig. 7. It is noted that the biaxial stress would reach maximum at specific biaxial strain, beyond that the biaxial stress will start to decrease. Fig. 8(a) and (b) show the snapshots of atomic displacements between two consecutive loading strain states, one is at small deformation and the other is before and after the stress drop. It is clear to notice that most of the deformation is accomplished by the atomic movement at the grain boundaries from equilibrium to 0.5% biaxial strain, which implies the amorphous grain boundary structure is more compliant than single crystalline grain structure. However, significant atomic displacements appear not only at the grain boundaries but also inside the grains before and after the maximum biaxial stress, which indicates that both the grain boundary sliding and some local structures, e.g., dislocations and stacking faults, emerging inside the grains. In order to recognize the complex local structure involving considerable number of atoms, the analysis based on Common Neighborhood Parameter [Tsuzuki, Branicio, Rino (2007)], which combines the advantages of the Common Neighbor Analysis (CNA) and the Centrosymmetry Parameter (CSP) methods into one parameter, is presented in Fig. 9 (a)-(c). Atoms are colored by the CNP values from 0\AA^2 in the fcc structure, to 4.4\AA^2 in the stacking fault, to 11\AA^2 at the dislocation core. It is observed that a lot of stacking faults and some dislocations appear inside the grains at 5% strain while most grains

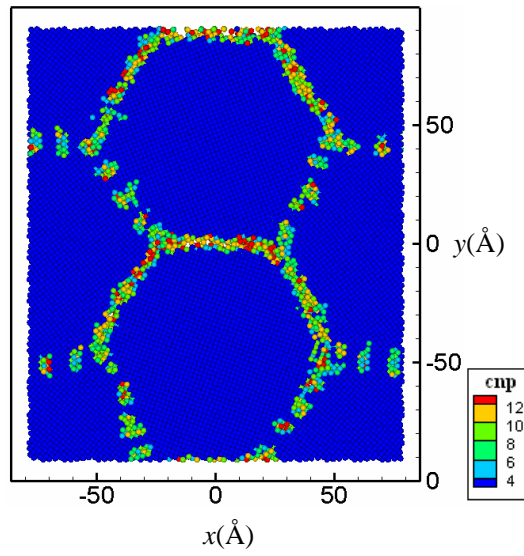


(a)

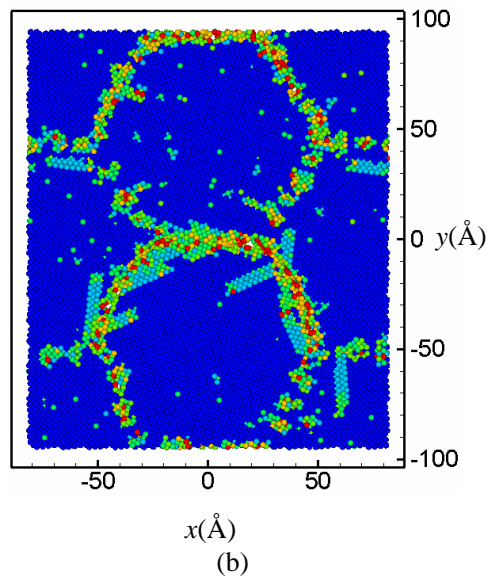


(b)

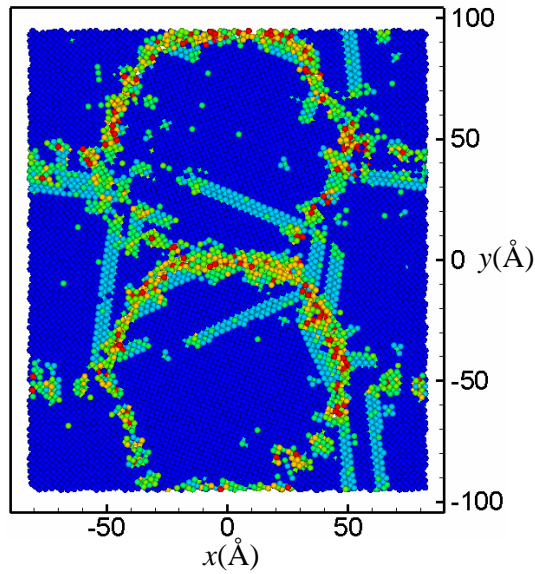
Figure 8: Snapshot of atomic displacement for polycrystalline nanofilm with grain size of 52.18\AA and film thickness of 36.15\AA , (a) at small deformation, from 0 to 0.5% strain, (b) before and after the biaxial yield stress, from 4.5% to 5% strain.



(a)



(b)



(c)

Figure 9: The atomic structure colored by CNP value under different biaxial loading strains. (a) 0.5%, (b) 4.5% and (c) 5%.

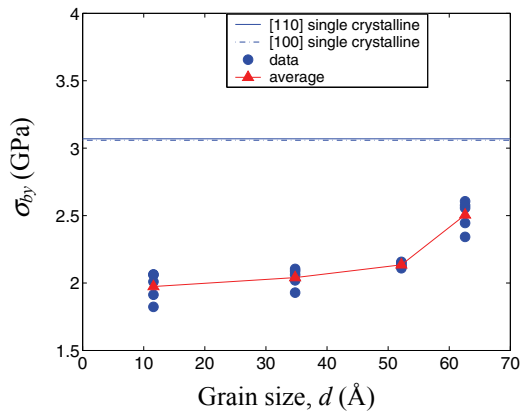


Figure 10: Size dependences of biaxial yield stresses on the grain sizes of polycrystalline nanofilms.

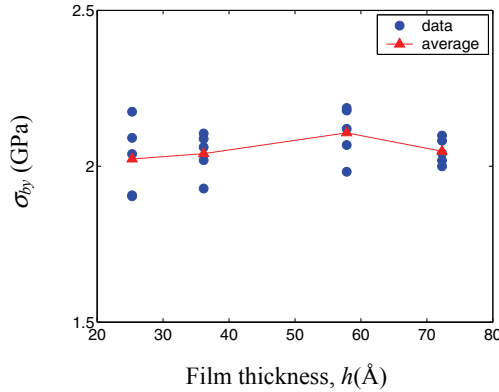


Figure 11: Size dependences of biaxial yield stresses on the film thicknesses of polycrystalline nanofilms.

remain as fcc crystal structure at 0.5% strain. Thus, the maximum biaxial stress is denoted as biaxial yield stress, σ_{by} .

The size dependences of biaxial yield stresses for different grain sizes and film thicknesses are shown in Fig. 10 and 11. It is noticed that the biaxial yield stresses increase as the grains become larger. Moreover, single crystalline nanofilm with out-of-plane normal direction fixed at the [001] direction are also loaded biaxially along $x[100]$, $y[010]$ and $x[110]$, $y[-110]$. It is observed that the biaxial yield stress for single crystalline nanofilms would be higher than the textured polycrystalline nanofilms. For single crystalline nanofilm, the stress drop is solely due to the dislocation nucleation. However, the dominant mechanisms for the plastic deformation in textured polycrystalline nanofilm is caused by the grain boundary sliding, stacking fault and dislocation nucleation inside grains, which would be easier to induce the plastic deformation. Hence, the inverse Hall-Petch effect becomes prominent in polycrystalline nanofilm. Besides, it is noted that the size dependence of the biaxial yield stress on the film thickness is not so pronounced.

4 Concluding Remarks

In this work, molecular dynamics approach combining with parallel computing scheme is employed to study the mechanical properties of textured polycrystalline nanofilms in order to clarify the size effect of microstructure and film thickness. The arrangements of the grain crystallographic orientations are random with out-of-plane normal direction fixed at [001] direction. The size dependences of elas-

tic and plastic properties for the infinite nanofilm under simple tension and biaxial loading are systematically examined, respectively. From MD simulation results, it is learned that the elastic and plastic properties of textured polycrystalline nanofilms show some dependent on the grain size and the film thickness. It is noticed that most of the deformation is accomplished by the atomic movement at the grain boundaries at small deformation, which implies the amorphous grain boundary structure is more compliant than single crystalline grain structure. It is also observed from the atomic displacement between two loading steps, before and after the biaxial yield stress, that both the grain boundary sliding and the dislocation emerging inside the grains are the dominant mechanisms for the plastic deformation, and thus, the inverse Hall-Petch effect becomes prominent in polycrystalline nanofilm.

Acknowledgement: This research work is supported by National Science Council of Taiwan under the grant NSC 97-2221-E-194-015 and NSC 98-2221-E-194-012-MY2. The support of AFOSR under contract No. FA2386-09-1-4152 AOARD 094152 is also acknowledged.

References

- Baral, D.; Ketterson, J. B.; Hilliard, J. E.** (1985): *J. Appl. Phys.* 57, 1076.
- Chang, I-L.; Chen, Y.-C.** (2007): *Nanotechnology* 18, 315701.
- Choi, Y.; Suresh, S.** (2002): *Acta Mater.* 50, 1881.
- Choi, Y. W.; Van Vliet, K. J.; Li, J.; Suresh, S.** (2003): *J. Appl. Phys.* 94, 6050.
- Cuenot, S.; Fretigny, C.; Champagne, S. D.; Nysten, B.** (2004): *Phys. Rev. B* 69, 165410.
- Daw, M. S.; Baskes, M. I.** (1984): *Phys. Rev. B* 29, 6443.
- Diao, J.; Gall, K.; Dunn, M. L.** (2004): *J. Mech. Phys. Solids* 52, 1935.
- Foiles, S. M.; Baskes, M. I.; Daw, M. S.** (1986): *Phys. Rev. B* 33, 7983.
- Hurley, D. C.; Tewary, V. K.; Richards, A. J.** (2001): *Thin Solid Films* 398, 326.
- Kalkman, A. J.; Verbruggen, A. H.; Janssen, G. C. A. M.** (2001): *Appl. Phys. Lett.* 78, 2673.
- Petersen, K.; Guarnieri, C.** (1979): *J. Appl. Phys.* 50, 6761.
- Renault, P.O.; Le Bourhis, E.; Villain, P.; Goudeau, P.; Badawi, K. F.; Faurie, D.** (2003): *Appl. Phys. Lett.* 83, 473.
- Ruud, J. A.; Jervis, T. R.; Spaepen, F.** (1994): *J. Appl. Phys.* 75, 4969.

Schiotz, J.; Jacobsen, K. W. (2003): Science 301, 1357.

Son, D.; Jeong, J.; Kwon, D. (2003): Thin Solid Films 437, 182.

Streitz, F. H.; Sieradzki, K.; Cammarata, R. C. (1990): Phys. Rev. B 41, 12285.

Tsuzuki, H.; Branicio, P. S., Rino, J. P. (2007): Structural characterization of deformed crystals by analysis of common atomic neighborhood. *Computer Physics Communications*, vol. 177, pp. 518-523.

Tracy, D. P.; Knorr, D. B. (1993): J. Electron. Mater. 22, 611.

Van Swygenhoven, H.; Derlet, P.; Caro, A.; Farkas, D.; Caturla, M.; Díaz de la Rubia, T. (2001): Mat. Res. Soc. Symp. 634, B5.5.1.

Villain, P.; Goudeau, P.; Renault, P. O.; Badawi, K. F. (2002): Appl. Phys. Lett. 81, 4365.

Yamakov, V.; Wolf, D.; Salazar, M.; Phillpot, S. R.; Gleiter, H. (2001): Acta Mater. 49, 2713.

Yamakov, V.; Wolf, D.; Salazar, M.; Phillpot, S. R.; Mukherjee, A. K.; Gleiter, H.D. (2002): Nat. Mater. 1, 1.

Yamakov, V.; Wolf, D.; Salazar, M.; Phillpot, S. R.; Mukherjee, A. K.; Gleiter, H.D. (2004): Nat. Mater. 3, 43.

Yang, W. M. C.; Tsakalakos, T.; Hilliard, J. E. (1977): J. Appl. Phys. 48, 876.